



Research Article

# Niclosamide and dichlorphenamide: new and effective corrosion inhibitors for carbon steel in 1M HCl solution



A. S. Fouda<sup>1</sup> · H. S. El-Desoky<sup>2</sup> · M. A. Abdel-Galeil<sup>2</sup> · Dina Mansour<sup>1</sup>

Received: 14 October 2020 / Accepted: 4 January 2021 / Published online: 8 February 2021

© The Author(s) 2021 [OPEN](#)

## Abstract

This research demonstrates the effect of some amide compounds (1 and 2) as corrosion inhibitors on C-steel in 1.0 M of hydrochloric solutions utilizing mass reduction studies, electrochemical [potentiodynamic (PP), AC impedance measurements (EIS), electrochemical frequency modulation] techniques, and surface checks were used to illustrate the importance of amide compounds to the corrosion protection process of C-steel. The tests displayed that the inhibition efficiency (IE%) augmented with increase in amide dose but reduced with growth of temperature. The highest inhibition efficiency is 99% for compound (1) and 98.8% for compound (2) at maximum dose tested (50  $\mu\text{M}$ ) by polarization method. PP data show that these compounds affect both cathodic and anodic processes (i.e. mixed type) and were adsorption on the carbon steel obeying Langmuir adsorption isotherm. The EIS results indicate that the changes in impedance parameters are related to the adsorption of amides on the alloy surface. Scanning of electron microscopy, energy transmitted X-ray—Atomic force microscopy studied the morphology of inhibited C-steel.

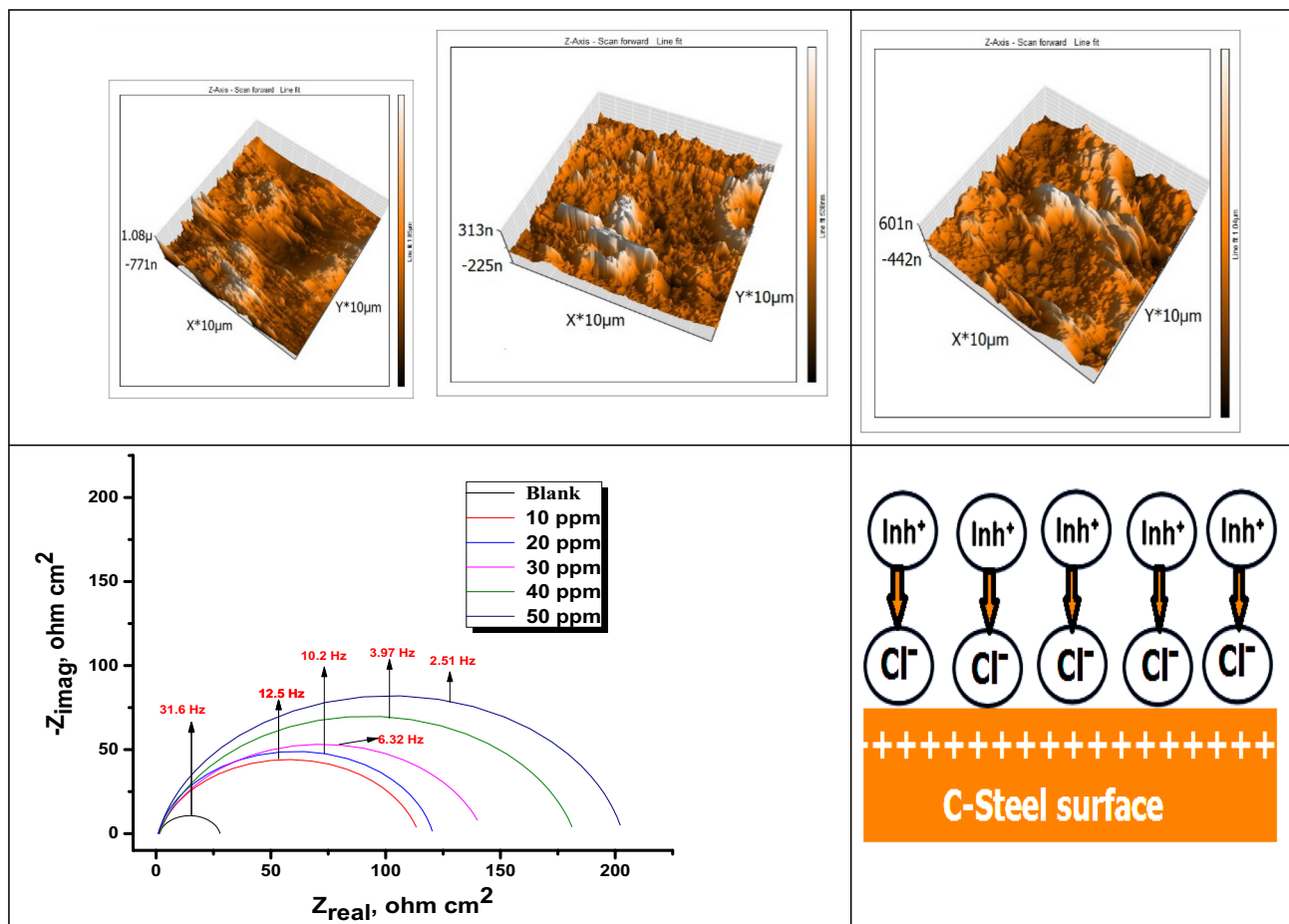
---

✉ A. S. Fouda, [asfouda@hotmail.com](mailto:asfouda@hotmail.com) | <sup>1</sup>Department of Chemistry, Faculty of Science, Mansoura University, Mansoura 35516, Egypt. <sup>2</sup>Department of Chemistry, Faculty of Science, Tanta University, Tanta 31527, Egypt.



SN Applied Sciences (2021) 3:287 | <https://doi.org/10.1007/s42452-021-04155-w>

Graphic abstract



**Keywords** C-steel corrosion · Amide derivatives · HCl · AFM · SEM · EDX

**1 Introduction**

Due to their environmental threat, the utilized of toxic materials as inhibitors has been restricted, so there is good interest in changing harmful inhibitors with impact non-hazardous substitutes [1–9]. In several industries corrosion inhibitors have been broadly research to minimize the dissolution rate of metal products in contact with destructive environment [10–14]. The high efficiency of corrosion inhibitors was correlated with their capability to adsorb on surface of metal [15]. Adsorption will also be based on the theoretical contact of the inhibitor’s π-orbitals with the surface atoms orbitals. This interaction causes greater adsorption on the C-steel surface, resulting in film-protective corrosion [16]. Organic compounds containing N, O, S heteroatoms and π electrons in their molecules are extensively used in the protection of metals and alloys

[17, 18] and are considered as effective corrosion inhibitors [19, 20]. It is noteworthy that a vast majority of these compounds e.g. pyridines, furans, imidazoles, thiophenes, isoxazoles, etc. have considerable similarity with the substructures of many of the commonly used drugs. This feature has prompted scientists across the globe to investigate the applicability of drugs as corrosion inhibitors. Bearing non-toxic characteristics and negligible negative environmental impact, drugs (chemical medicines) have emerged as suitable candidates to replace the conventionally used toxic corrosion inhibitors [21] (Table 1).

So, the goal of this study is to learn how these amide compounds (drugs) often influence corrosion protection of C-steel through data obtained from electrochemical and mass reduction tests, in addition to analyze the metal surface by several techniques (SEM, EDX and AFM).

## 2 Experimental

### 2.1 Composition of carbon steel samples

We used: a—Working electrode manually made from cylindrical steel material (Table 2).

b—Carbon steel pieces: which have a rectangular design with an area  $1 \text{ cm}^2$ .

### 2.2 Chemicals

a—HCl (BDH grade) b—amide derivatives recorded in Table 3

b—The inhibitors utilized with different doses ranged from 10 to 50  $\mu\text{M}$ . 1000  $\mu\text{M}$  stock solutions from the utilized inhibitors were prepared by dissolving the convenient weights (1 g) of used amides in bidistilled water, the other doses of amides (10–50  $\mu\text{M}$ ) were prepared by dilution with bidistilled water. All the materials utilized were of AR grade and used as received. The structure formulas of the examined inhibitors were given in Table 3.

### 2.3 Structure confirmation of amide compounds by Fourier transfer infrared spectroscopy (FTIR)

The confirmation and approval of the chemical composition for the amide compounds was performed by utilizing FTIR spectroscopy which taken by utilized Thermo Fisher Nicolet IS10, in the attendance of (KBr).

### 2.4 Mass reduction (MR) test

The standard method for assessing the rate of corrosion and inhibition efficiency (% IE) is a method of mass reduction in which the piece of metal with a scale of  $2 \text{ cm}^2$ . "The samples are cut and polished as before, then we wash the samples with double distilled water, dried, and weighed, and put them in solutions prepared from different concentrations of amide compounds from 10 to 50  $\mu\text{M}$  in a baker containing 1.0 M HCl and changing quantities of amide compounds for 3 h. This occurs in the attendance of 1.0 M HCl to compare with a sample that was placed

**Table 2** Chemical conformation of C-steel

Elements	C	Mn	P	Si	Fe
Weight %	0.20%	0.90%	0.007%	0.002%	Rest

**Table 1** Chemical structures, names, nature of metals and electrolytes, and maximum inhibition efficiencies of the drugs used as corrosion inhibitors for mild steel in acid solution

Drug name and structure	Nature of metal/electrolyte	Mode of adsorption	Maximum efficiency/Conc.	Ref.
Donaxine	Mild steel/1 M HCl	Mixed type/Langmuir adsorption isotherm	98% at 7.5 mM	[22]
Penicillin G (X, Y = H); ampicillin (X = H, Y = -NH <sub>2</sub> ); amoxicillin (X = -OH, Y = -NH <sub>2</sub> )	Carbon/1 M HCl	Mixed type/Langmuir adsorption isotherm	98.4%, 95.5% and 93% at 10 mM for Pen, Amp and Amo, respectively	[23]
Atenolol	Mild steel/1 M HCl	Mixed type/Langmuir adsorption isotherm	93.8% at 300 ppm	[24]
Cephalothin	API 5L X52/1 M HCl	Langmuir adsorption isotherm	92% at 600 ppm	[25]
Telmisartan	Mild steel/1 M HCl	Mixed type/Temkin adsorption isotherm	97.39% at 125 mg L <sup>-1</sup>	[26]
Metronidazole	Mild steel/0.5 M HCl	Anodic type/Temkin adsorption isotherm	80.01% at 10 $\mu\text{M}$	[27]
Tinidazole	Mild steel/1 M HCl	Mixed type/Langmuir adsorption isotherm	90% at 400 ppm	[28]
Cimetidine	Mild steel/1 M HCl	Mixed type/Langmuir adsorption isotherm	95.6% at 500 ppm	[29]
25[25][25][25] Amodiaquine	Mild steel/1 M HCl	Langmuir adsorption isotherm	44.33% at 0.006 M	[30]
Sparfloxacin	Mild steel/2.5 M HCl	Langmuir adsorption isotherm	97.47% at $12 \times 10^{-4}$ M	[31]
Fluconazole	Mild steel/2.5 M HCl	Anodic type/Langmuir adsorption isotherm	96% at 0.30 mM	[32]
Piperacillin Sodium	Mild steel/1 M HCl	Mixed type/Langmuir adsorption isotherm	93% at $7.2 \times 10^{-4}$ M	[33]
Ciprofloxacin	Mild steel/1 M HCl	Langmuir adsorption isotherm	86% at $2.570 \times 10^{-3}$ M	[34]

in a solution of 1.0 M hydrochloric acid without added amide compounds. The samples are weighed, and then placed again in their solutions, then samples were taken away and handled following the process cleared in ASTM term G1-90 [37]. The temperature ranges from 30 to 500 C°. Shined well and was inserted in a baker containing 1.0 M HCl and changing quantities of amide compound inhibitors for 3 h).

## 2.5 Electrochemical tests

### 2.5.1 Potentiodynamic polarization (PP) measurements

The measurements shifted automatically of PP from – 700 to + 700 mV vs. (Eocp). The measurement has been checked at a scan rate of 1 mVs<sup>-1</sup>.

### 2.5.2 Electrochemical impedance spectroscopy (EIS) tests

All open-circuit tests with EIS performed the experiment by using AC signals ranging from 100 k Hz to 0.1 Hz with an amplitude of peaks 10 mV at OCP.

### 2.5.3 Electrochemical frequency modulation (EFM) tests

EFM experiment utilized the signal with a capacity of 10 mV through two sinus waves from 2 to 5 Hz, and the choice depends on three arguments. This technology is fast and not destructive. Corrosion current density (icorr),

causal factors CF2 and CF3, and Tafel slopes ( $\beta_a$  and  $\beta_c$ ) were determined through the higher peaks [38]. In electrochemical tests, the device utilized in the EFM methods was Gamry Potentiostat/Galvanostat/ZRA (PCI4-G750). Gamry includes DC105 DC corrosion program and EIS300 EIS program, the EFM140 for EFM program, as well as a computer for data collection. Echem Analyst version 5.5 was utilized to plot, calculate data.

## 2.6 Surface morphology

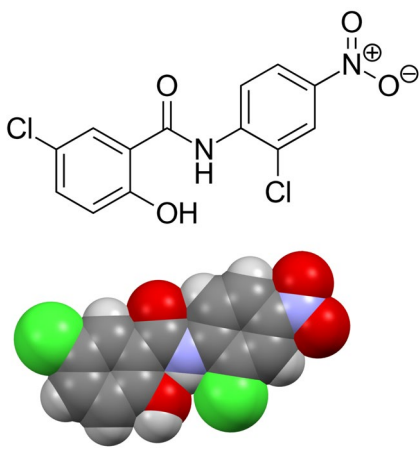
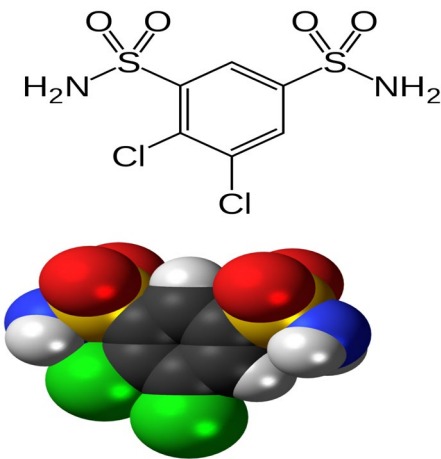
### 2.6.1 Fourier transfer infrared (FTIR) spectroscopy

FTIR utilized for determination the functional groups present in amide compounds after adding it at a higher concentration of 50  $\mu$ M and after adding it in a solution of 1.0 M hydrochloric acid with C-steel metal coupon three hours, a FTIR analysis used through (FT/IR-4100typeASerial B117761016).

### 2.6.2 SEM–EDX analysis

the morphology of C-steel metal samples was tested before and after being dipping in 1.0 M hydrochloric acid in the existence and non-existence of amide compounds (50  $\mu$ M) for 3 hours using Cu-tube (Cu Kal,1 = 1,54,051 Ao) with a Philips X-ray diffract meter (pw-1390). SEM, JOEL, JSM-T20, Japan.

**Table 3** Chemical structure of amide compounds [35, 36] which utilized as inhibitors

Compound	1	2
Names	Nicosamide drug	Dichlorphenamide drug
Structure		
Mol. weight	327.11 g/mol	305.2 g/mol
Mol. formula	C13H8Cl2N2O4	C6H6Cl2N2O4S2
IUPAC name	5-chloro-N-(2-chloro-4-nitrophenyl)-2-hydroxybenzamide	4,5-dichlorobenzene-1,3-disulfonamide

### 2.6.3 Atomic force microscopy (AFM) analysis

AFM, technique was studied to obtain the morphological properties of the C-steel surface. This exam occurs in 1.0 M of HCl acid in the lack of amide compound drugs and in the existence of the maximum dose of amide compound drugs. AFM was carried out in contact mode utilizing fractions of a nanometer, more than 1000 times excellent than the optical diffraction limit.

### 2.7 Quantum calculations

Gaussian version 4.4.0 used density functional theory (DFT) [39] to measure the quantum chemical parameters and indexes.

### 2.8 Monte Carlo (MC) Simulation

MC simulations were achieved using Materials Studio 7.0 (Accelrys Inc., San Diego, "CA, USA) in a simulation box with periodic boundary conditions. A pure iron crystal was introduced and cleaved along the most stable (less energy) plane (110) constructing a 30 Å vacuum slab. The plane surface of Fe (110) has been relaxed by decreasing its energy; this step has been followed by extending the surface of Fe (110) to a super cell (10/10). The simulation analysis was performed in a test box containing the simulated corrosive species and one molecule of each inhibitor using the Monte Carlo quest and assigning the COMPASS force field known as a high-quality force field to combine parameters of inorganic and organic materials" [40].

## 3 Results data and discussion

### 3.1 MR test

The MR which calculated from Eq. 1 is as follows:

$$\Delta W = \frac{W_1 - W_2}{a} \quad (1)$$

where  $W_1$ ,  $W_2$  the weights of the C-steel specimens earlier and later reaction with solution, respectively. The IE% was measured using Eq. 2:

$$IE\% = \left[ 1 - CR_{inh.}/CR_{free} \right] \times 100 \quad (2)$$

where  $CR_{free}$  and  $CR_{inh}$  are the corrosion rates without and with inhibitors, respectively.

Figure 1 shows the calculated MR for C-steel in the attendance and absence of altered doses ranging from 10 to 50  $\mu$ M for compound 1, similar curves gotten from other compound (not display). By increasing the temperature,

the IE% was lowered, while corrosion rate (C.R) increased (Fig. 1) for amide compound (1) which is the best effect. The increased IE% with raised dose of amide compounds can be qualified to the creation of a layer of the inhibitors on the C-steel surface by adsorption. This layer is formed by the pairs of free electrons present on the oxygen and nitrogen atoms in the amide compound molecules as well as the  $\pi$ -electrons of the aromatic rings" [17]. Decrease in the IE% with a higher temperature (Table 4) may likely be due to increased rate of desorption meaning that is physical adsorption, the order of IE% was as follows:  $1 > 2$ .

### 3.2 Temperature influence on corrosion process

The important factor that determine the rate of reaction and the type of adsorption is activation energy  $E_a^*$  which can be calculated from Eq. (3):

$$\log C.R = \log A - E_a^*/2.303RT \quad (3)$$

where A Arrhenius constant. Arrhenius plots are illustrated in Fig. 2 [ $\log$  (C.R) against  $1/T$ ], in which the energy of the activation is derived from the slopes of straight lines [ $-E_a^*/2.303R$ ]. "The analysis of the results was obtained in Table 5, it implies surface reaction dominates the overall activity, since the corrosion process ( $E_a^*$ ) is over ( $20 \text{ kJ mol}^{-1}$ ) and increase in the activation energy by increasing the dose of amide compounds. This increase is due to the adsorption nature of amide compounds on the C-steel and corresponds to the physical adsorption of the amide compound drugs [41]. Using the transitional state equation, the changes in entropy and enthalpy were calculated. The increase in activation enthalpy ( $\Delta H^*$ ) and the increase in entropy ( $\Delta S^*$ ) for C-steel corrosion in 1.0 M HCl were calculated using the following equation from the theory of transition state [42].

$$\log(C.R./T) = [\log(R/Nh) + DS_a^*/2.303R] - DH_a^*/2.303RT \quad (4)$$

where symbol "h" equal Planck's constant. Graph of  $\log$  (C.R/T) versus ( $1/T$ ) for unprotected C-steel at 1.0 M HCl and in the existence of amide compound inhibitors Fig. 3 includes straight lines with slope equal ( $-\Delta H^*/2.303R$ ) and an intercept equal ( $\log R/Nh - \Delta S^*/2.303R$ ) from which  $\Delta H^*$  and  $\Delta S^*$  data were calculated and defined in Table 6). Negative data of ( $\Delta H^*$ ) on the C-steel surface, which in turn indicates that the reaction that occur in the dissolution process is exothermic and it is known that they can be applied to chemical adsorption and physical adsorption [43–48]. The mean values ( $\Delta S^*$ ) are high and negative; this implies that the activated complex is an interaction rather than a dissociation phase in the rate-determining stage.

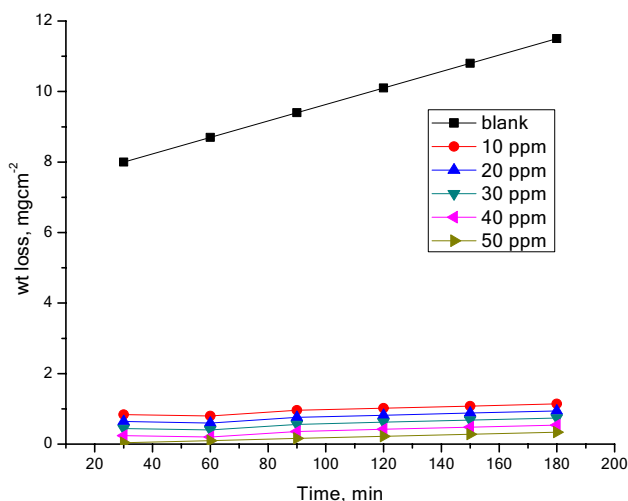


**Fig.1** Time-MR curves of C-steel in hydrochloric solution existence and absence of various doses of compound (1) at 30 °C

### 3.2.1 Adsorption isotherm behavior

Figure 4 shows the  $C_{inh}/\theta$  relationship dependency for compound 1, as a result of the doses of amide inhibitors ( $C_{inh}$ ) obeying Langmuir isotherm adsorption.

$$C/q = 1/K_{ads} + C \tag{5}$$

where  $K_{ads}$  is the equilibrium adsorption constant intricate in chemical reaction

$$K_{ads} = (1/55.5) \times \exp(-\Delta G_{ads}^0/RT) \tag{6}$$

In which  $-\Delta G_{ads}^0$  the regular free adsorbent, 55.5 dosage of molar water in solution. Data pattern showed that the negative sign of  $\Delta G_{ads}^0$  owing to the spontaneous adsorption on the metal surface [49]

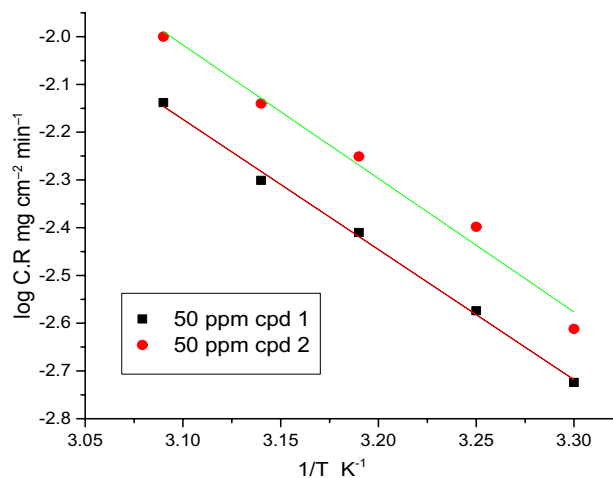


**Fig.2** Log C.R versus 1/T of investigated amide inhibitors with concentration 50 μM and free sample at temperature range 30–50 °C

Table 7 shows the adsorption parameters for the obtained amide inhibitors. the results obtained from free energy confirm that the type of adsorption incident is physical and chemical adsorption as it is known that negative values when they are higher than 20 kJ/mol and lower than 40 kJ/mol, using the next equation, the determined ( $-\Delta H_{ads}^0$ ) and ( $-\Delta S_{ads}^0$ ):

$$\Delta G_{ads}^0 = \Delta H_{ads}^0 - T\Delta S_{ads}^0 \tag{7}$$

and this by plotting  $\Delta G_{ads}^0$  against T to find these data [ $-\Delta H_{ads}^0$  and ( $-\Delta S_{ads}^0$ )] Fig. 5. The value of enthalpy is negative, which means that adsorption molecules are exothermic [50]. The values  $\Delta H_{ads}^0$  are less than 100 kJ/mol, representative that the physisorption.

**Table 4** (IE %) at various doses of amide compounds of C-steel at 30-50 °C temperature range for 180 min. immersion from MR test

Inhibitor	Conc. μM	IE%				
		30 °C	35 °C	40 °C	45 °C	50 °C
1	10	90.09	89.42	85.64	83.77	80.47
	20	91.83	91.07	87.88	86.36	83.63
	30	93.57	92.73	90.15	88.96	86.79
	40	95.30	94.38	92.42	91.56	89.95
	50	97.04	96.03	94.69	94.16	93.11
2	10	85.74	84.13	80.22	78.57	77.89
	20	88.35	86.61	83.26	81.81	81.05
	30	90.96	89.09	86.29	85.06	84.21
	40	93.57	91.57	89.32	88.31	87.37
	50	96.10	94.05	92.35	91.55	90.53

**Table 5** Corrosion rate of investigated compounds and free sample at 180 min

Temp °C	C.R Free sample	C.R Cpd. 1 (50 μM)	C.R Cpd. 2 (50 μM)
30	0.0640 ± 0.002906	1.89 × 10 <sup>-3</sup> ± 2.31E-05	2.44 × 10 <sup>-3</sup> ± 3.21E-05
35	0.0672 ± 0.000203	2.66 × 10 <sup>-3</sup> ± 3.21E-05	4.00 × 10 <sup>-3</sup> ± 4.48E-05
40	0.0733 ± 0.000346	3.88 × 10 <sup>-3</sup> ± 3.46E-05	5.61 × 10 <sup>-3</sup> ± 3.46E-05
45	0.0856 ± 0.000208	5.00 × 10 <sup>-3</sup> ± 0.000318	7.22 × 10 <sup>-3</sup> ± 4.91E-05
50	0.1056 ± 0.000521	7.29 × 10 <sup>-3</sup> ± 0.000228	10.00 × 10 <sup>-3</sup> ± 0.00060

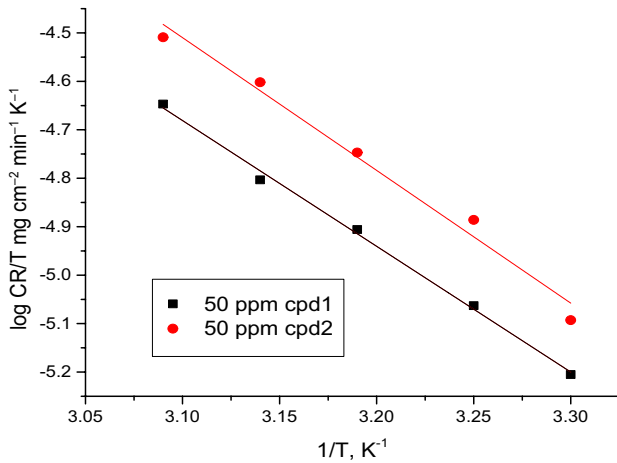


**Fig. 3** Log (C.R/T) versus 1/T of investigated amide compound inhibitors with concentration 50 μM and free sample at temperature range 30–50 °C

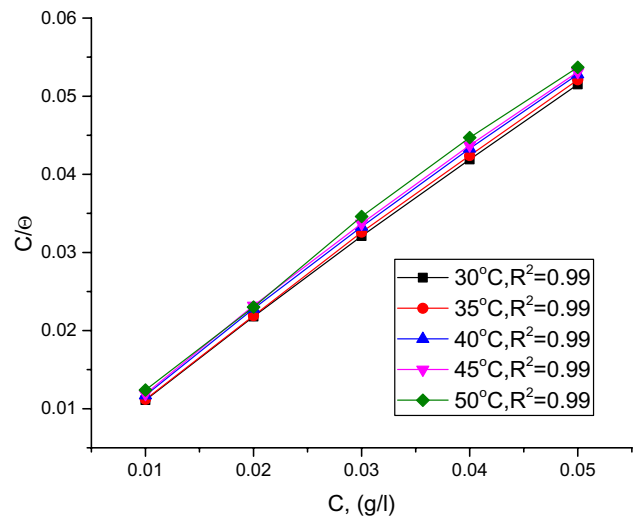


**Fig. 4** Langmuir isotherm adsorption of compound 1 at various temperatures on a C-steel at 1 M HCl

**Table 6** C-steel dissolution parameters when 50 μM of investigated amide compound inhibitors at 30–50 °C are absent and present

Inhibitor	Activation parameters		
	E <sub>a</sub> <sup>*</sup> kJ mol <sup>-1</sup>	-ΔH <sup>*</sup> kJ mol <sup>-1</sup>	-ΔS <sup>*</sup> J mol <sup>-1</sup> K <sup>-1</sup>
1 M HCl	19.8	17	211
1	55.1	50	130
2	52.7	52	121

### 3.3 Electrochemical measurements

#### 3.3.1 PP measurement

The influence of investigated compounds on the corrosion and inhibition of carbon steel in 1 M HCl solutions was studied. Figures 6 and 7 show the PP curves of carbon steel in uninhibited and inhibited solutions by various doses of

the used amide compounds. The various electrochemical corrosion parameters and the IE% estimated using Eq. (7). Values of polarization parameters; corrosion potential E<sub>corr</sub>, Tafel slopes, β<sub>c</sub>, β<sub>a</sub>, (are measure of the symmetry of the activation barrier for the cathodic and anodic reaction) and corrosion current density (I<sub>corr</sub>) as well as IE%, θ are listed in Table 8. The shape of the cathodic and anodic curves did not change much with the addition of these compounds, but β<sub>c</sub> is slightly higher than β<sub>a</sub>, and this suggests that the used inhibitors affect both cathodic and anodic processes (mixed one), with predominant cathodic effect. E<sub>corr</sub> values showed a slight shift towards cathodic regions with the addition of the various doses of amides, suggesting that the effect of amides is more pronounced on the cathodic process. In the previous studies [51, 52] if the minimum shift in E<sub>corr</sub> was ± 85 mV, the inhibitor is considered as cathodic or anodic type. In the present study, the maximum shift was 50–62 mV for the two compounds, indicating that the utilized amide compounds are mixed-type inhibitors. The cathodic curves are almost having parallel Tafel lines. This indicates that in the presence of these compounds there is no modification in the mechanism of H<sub>2</sub> evolution, and the inhibitor molecules only

**Table 7** Kinetic parameters of investigated compounds as a function of temperature for C-steel dissolution at 1 M HCl

Compound	Temp K	R <sup>2</sup>	K <sub>ads</sub> M <sup>-1</sup>	−ΔG <sup>°ads</sup> kJ mol <sup>-1</sup>	−ΔH <sup>°ads</sup> kJ mol <sup>-1</sup>	−ΔS <sup>°ads</sup> J mol <sup>-1</sup> K <sup>-1</sup>
1	303	0.99	740	26.7	21.1	189.8
	308	0.99	709	26.8		
	313	0.99	507	26.9		
	318	0.99	444	27.1		
	323	0.99	418	27.2		
2	303	0.99	462	25.6	14.5	166.6
	308	0.99	452	25.8		
	313	0.99	357	26.0		
	318	0.99	327	26.2		
	323	0.99	322	26.3		

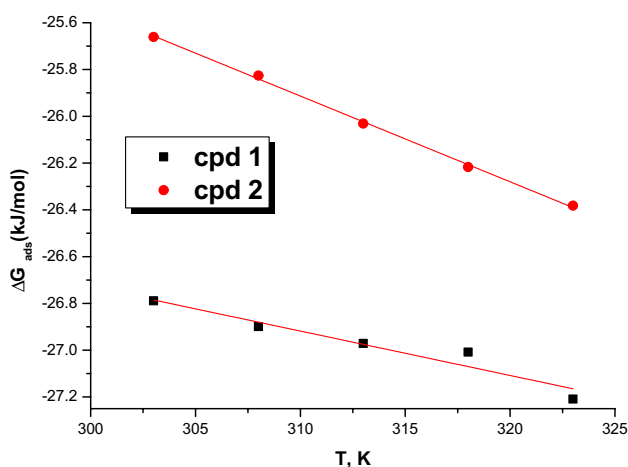


**Fig. 5** ΔG<sup>°ads</sup> versus T diagrams obtain from Langmuir

block the active sites of hydrogen evolution by adsorption on steel surface. In the case of anodic parts of the curves, the anodic reaction of corrosion is markedly suppressed in the presence of inhibitors, but there is stronger inhibitive effect on the cathodic reaction (Table 8) than on the anodic one. The data in Table 8 indicate that the *I*<sub>corr</sub> is reduced as the inhibitor does increase and hence, IE% increased and show reasonable agreement with the results obtained by other techniques.

### 3.3.2 Electrochemical impedance spectroscopy (EIS) tests

Figures 8 and 9 show C-steel Nyquist and Bode diagrams, given at OCP both existence and nonexistence of altered doses of amide compound (1) at 30 °C, respectively. Similar curves for amide compound (2), not displayed. “The impedance spectra show that the diameter increases as the dose of amide studied rises. The interfacial capacitance

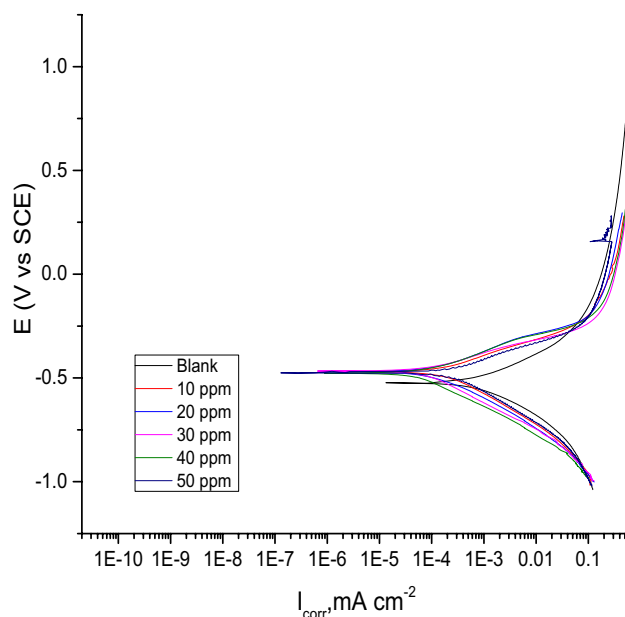


**Fig. 6** Polarization curves for the dissolution of C-steel in 1.0 M HCl in the presence and absence of various doses of compound (1)

*C*<sub>dl</sub> values can be estimated from CPE parameter (*Y*<sub>0</sub> and *n*) is defined in Eq. 8:

$$C_{dl} = Y_0(\omega_{max})^{n-1} \tag{8}$$

where *Y*<sub>0</sub> is a proportional factor while *n* is the CPE exponent which can be explained as a degree of surface inhomogeneity (− 1 < *n* < 1). When *n*=0, CPE represents a resistance, when *n*=1 a capacitance, when *n*=− 1, an inductance and when *n*=0.5, a Warburg impedance. In our study, values of *n* with and without amides range from 0.836 to 0.798. The deviation from unity (ideal capacitive behavior) is due to the presence of surface



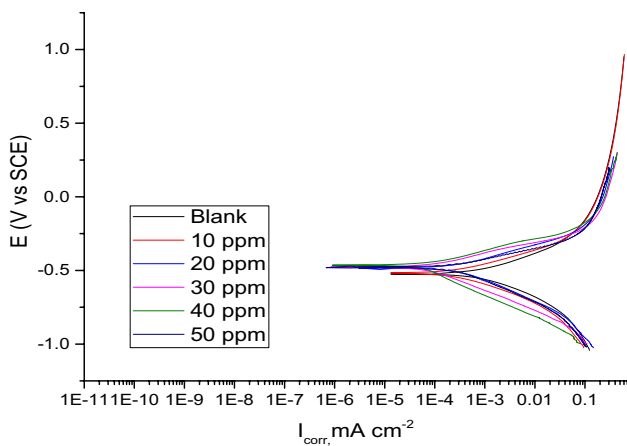


**Fig. 7** PP diagrams for the dissolution of C-steel in 1.0 M HCl where various amounts of compound 2 are absent and present

inhomogeneity and surface roughness [53]. Using Eq. 8. “The obtained diagrams for different inhibited solutions by amide compounds are very similar for that recorded in the absence of amide, this indicates that the interface mechanism is no modified [43, 54, 55]. They present a single depressed capacitive semi-circle. The impedance parameters obtained by fitting the EIS data Fig. 10 by equivalent circuit using Zview software, containing the electrolyte resistance ( $R_s$ ), the charge transfer resistance ( $R_{ct}$ ) and the constant phase element (CPE). Table 9 lists the values of parameters like  $R_s$ ,  $R_{ct}$ ,  $n$ ,  $Y_0$  by EIS fitting as well as the derived parameters  $Cdl$  and  $IE\%$ . The data of Table 9 demonstrate the data of  $R_{ct}$  increase with raising the dose of the amide compounds and this pointed to the rise in  $IE\%$ . This might be because of the rise of the thickness of the adsorbed layer by raising the amide compound

doses, indicating that the recovery of the metal surface is performed by the adsorption of amide molecules. The increased surface smoothness in presence of amides can also be supported by Bode plots. One can see from Bode plots with and without inhibitor that the deviation from ideal capacitive behavior is more effective in the absence of inhibitor. The slope of the phase angle values increased significantly in presence of inhibitor owing to the formation of a protective film. Moreover, the increased values of phase angles are more effective at high inhibitor dose. The decrease in  $Cdl$  with rise of amide dose, this behavior can be due to a rise in the thickness of the double layer and/or a diminution in local dielectric constant, this variation explained the inhibitor molecule function by adsorption at electrode/solution interface [44]. The  $\%IE$  and the  $(\theta)$  from the impedance tests were obtained by:

$$\%IE = \theta \times 100 = \left[ 1 - \frac{R_p^o}{R_p} \right] \times 100 \tag{9}$$

where  $R_p^o$  and  $R_p$  are the resistances unprotected and protected amide, individually.

It is observed that in the Bode plots in the presence of compound (1) there is an increase in the low frequency impedance modulus, which indicates the adsorption of compound (1) and improving corrosion resistance of C-steel. The increase of phase angle in the presence of compound (1) i.e. approaching towards  $-90^\circ$  indicates that there is only one-time constant and is related to electrical double layer formation at surface/solution interface [45].

**Table 8** Effect of compounds 1&2 doses on ( $E_{corr}$ ), ( $i_{corr}$ ), ( $\beta_c$ ,  $\beta_a$ ), ( $\theta$ ) and ( $IE\%$ ) of C-steel in 1 M of HCl at 30 oC

[Inh.] $\mu M$	$-E_{corr}$ mV versus SCE	$i_{corr}$ $\mu A cm^{-2}$	$\beta_c$ mV dec <sup>-1</sup>	$\beta_a$ mV dec <sup>-1</sup>	$\theta$	$IE\%$
<i>Blank</i>						
–	525 ± 0.230	945 ± 0.260	161.8 ± 0.230	145.7 ± 0.1764	–	–
<i>Comp. 1</i>						
10	459 ± 0.491	172.2 ± 0.233	143.6 ± 0.264	92.1 ± 0.1207	0.817	81.7
20	475 ± 0.346	94 ± 0.288	119.8 ± 0.260	62.9 ± 0.176	0.900	90.0
30	468 ± 0.375	69.5 ± 0.433	131.1 ± 0.233	71.9 ± 0.1733	0.926	92.6
40	459 ± 0.264	59.8 ± 0.375	133.3 ± 0.223	72.0 ± 0.264	0.936	93.6
50	462 ± 0.230	8.6 ± 0.435	77.9 ± 0.255	49.1 ± 0.1851	0.990	99.0
<i>Comp. 2</i>						
10	464 ± 0.145	181.8 ± 0.176	139.1 ± 0.375	90.3 ± 0.272	0.807	80.7
20	483 ± 0.088	134.8 ± 0.115	121.5 ± 0.178	85.7 ± 0.208	0.857	85.7
30	477 ± 0.260	69.8 ± 0.288	135.6 ± 0.145	79.2 ± 0.274	0.926	92.6
40	464 ± 0.218	53.6 ± 0.230	158.9 ± 0.152	79.2 ± 0.233	0.943	94.3
50	463 ± 0.251	9.6 ± 0.202	77.9 ± 0.232	45.8 ± 0.221	0.989	98.9

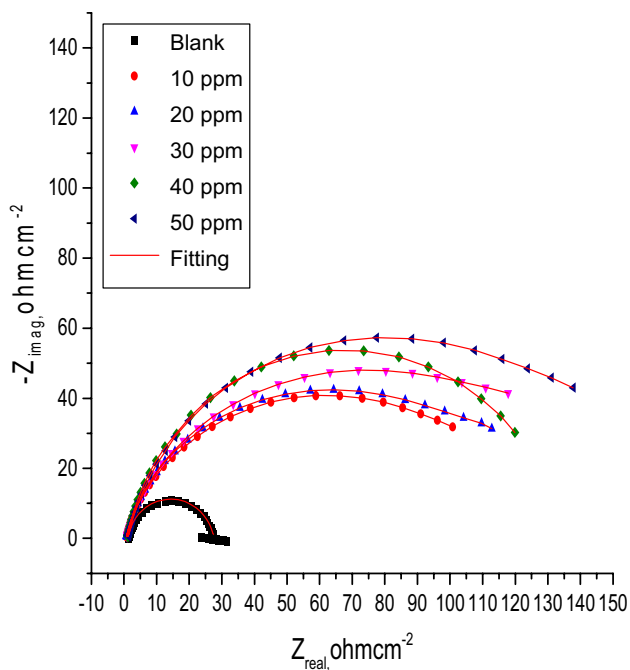


**Fig. 8** The Nyquist diagrams for the dissolution of C-steel in 1 M HCl in the presence and absence of altered doses of amide compound (1) at 30 °C

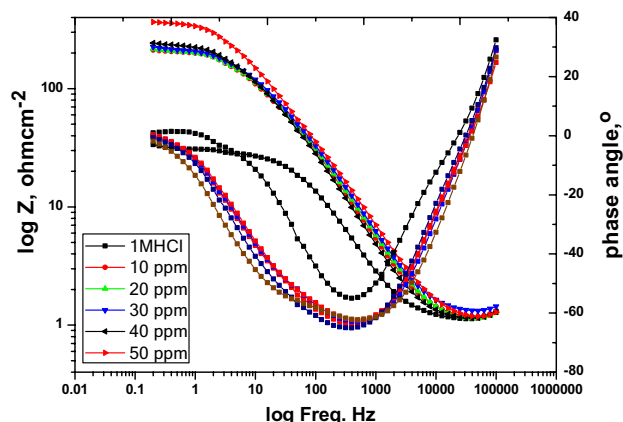


**Fig. 9** The Bode diagrams for the dissolution of C-steel in 1 M HCl in the presence and absence of altered doses of amide compound (1) at 30 °C

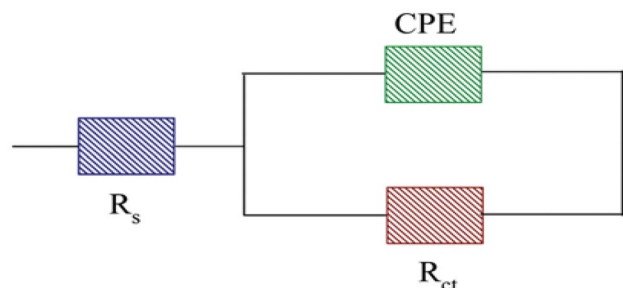


**Fig. 10** Equivalent circuit model represents the metal /solution interface

**Table 9** EIS parameters for the for the dissolution of C-steel in 1 M HCl in the attendee and lack of altered dosage of investigated amide compound drug at 30 °C

Conc. $\mu\text{M}$	$R_{ct}$ , $k\ \Omega\ \text{cm}^2$	$C_{dl}$ , $\times 10^{-4}$ , $\mu\text{F}\ \text{cm}^{-2}$	$\Theta$	IE%	
1 M HCl	$23.9 \pm 0.51$	$1.24 \pm 0.43$	–	–	
Comp.1	10	$95.1 \pm 0.55$	$1.15 \pm 0.29$	0.747	74.7
	20	$98.8 \pm 0.37$	$0.97 \pm 0.52$	0.757	75.7
	30	$110.6 \pm 0.46$	$0.89 \pm 0.49$	0.783	78.3
	40	$155.9 \pm 0.37$	$0.82 \pm 0.41$	0.846	84.6
	50	$180.1 \pm 0.38$	$0.71 \pm 0.55$	0.866	86.6
Comp. 2	10	$88.1 \pm 0.33$	$1.17 \pm 0.46$	0.727	72.7
	20	$97.1 \pm 0.42$	$1.11 \pm 0.31$	0.753	75.3
	30	$106.9 \pm 0.51$	$1.10 \pm 0.53$	0.775	77.5
	40	$117.1 \pm 0.22$	$0.79 \pm 0.45$	0.795	79.5
	50	$130.0 \pm 0.36$	$0.69 \pm 0.24$	0.815	81.5

### 3.3.3 Electrochemical frequency modulation (EFM) measurements

The tests of the EFM procedure demonstrated good agreement with the Tafel system of extrapolation for the rate of corrosion achieved [46]. “Fig. 11, indicates the EFM of C-steel in 1 M HCl solution and altered dose of amide (1). Similar spectra for amide (2), not display. The EFM parameters such as (CF-2 and CF-3), ( $\beta_c$  and  $\beta_a$ ) and ( $i_{corr}$ ) can be measured from the higher current peaks. Table 10 describes the measured parameters of kinetic corrosion at various dose of the studied amide compound drugs at 1 M HCl at 30 °C. The current corrosion densities reduction by raising the dose of the investigated amide drugs, as well as increasing the inhibition efficiency”. Using this technique, the following was extracted: With an increased concentration of amide compound drugs, there is a noticeable lowered in the intensity of the corrosion current and a clear increase in the %IE.

### 3.4 Scanning electron microscope (SEM) analysis

SEM micrographs obtained for C-steel samples with and without 50  $\mu\text{M}$  of investigated compounds are shown in Fig. 12. The blank image reveals a very rough and highly corroded surface in the absence of investigated compounds [47]. As can see from images in presence of compounds 1 and 2, the damage of the steel surface has diminished in the presence of inhibitors and rough, corroded steel surface displaces to much smooth.

### 3.5 Energy dispersion spectroscopy (EDX) analysis

The EDX were utilized to test the elements existence on the surface of C-steel with and without the 50  $\mu\text{M}$  amide

compounds shown in Fig. 13. In the blank diagram, the absence of oxygen peak, which reveals the dissolution of oxide layer. But in the presence of inhibitors an additional peak of oxygen from the inhibitors is observed, which confirms there is adsorption.

### 3.6 AFM tests

AFM in Fig. 14 measured the surface roughness of C-steel in 1.0 M HCl, attendance and absence of 50  $\mu\text{M}$ . Where, (a) blank, (b) C-steel with compound (1) 50  $\mu\text{M}$  and compound (2) 50  $\mu\text{M}$  C-steel [47]. The degree of roughness was shown in Table 11. As shown from the Table the surface became more smoother in presence of the extract than in its absence, due to the formation of a protective layer on metal surface and compound (1) became more smoother than compound (2).

### 3.7 FT-IR analysis

Figure 15 represents the FTIR of pure Niclosamide and Dichlorphenamide compounds. The frequency worth

of C=O stretch at  $1789\text{ cm}^{-1}$ . "The band at  $1634$  like C=C stretch. The band at  $1556$  is like N-H bend for amide. The band at  $1391\text{ cm}^{-1}$  is like  $-\text{CH}(\text{CH}_3)_2$  for Alkyls [1]. The band at  $1426\text{ cm}^{-1}$  is like  $=\text{C}-\text{O}-\text{C}$  sym. for Alkyls [1]. The band at  $1145\text{ cm}^{-1}$  is like C-O stretch [1]. The band at  $365\text{ cm}^{-1}$  is like C-Cl stretch [1]. Figure 16 shows the FT-IR spectra of pure Dichlorphenamide compound. The stretching -OH- frequency appears at  $3435\text{ cm}^{-1}$ , the stretching C=O frequencies appear at  $1690$ , the bending  $-(\text{CH}_3)_3$  frequency appears at  $1350\text{ cm}^{-1}$ , the bending C-O frequency appears at  $1178\text{ cm}^{-1}$  and  $1114\text{ cm}^{-1}$ , the stretching S=O frequencies appear at  $1038$ , the bending C-Cl frequency appears at  $897\text{ cm}^{-1}$ , the bending  $\equiv\text{C}-\text{H}$  bend frequency appears at  $650$ .

### 3.8 Quantum chemical calculations

Figure 17 represents the frontier molecular orbital density distribution for compound (1) and compound (2) (HOMO and LUMO). From density functional theory, the energy of EHOMO and ELUMO has important roles in predicting the adsorption centers in inhibitor molecules, as EHOMO

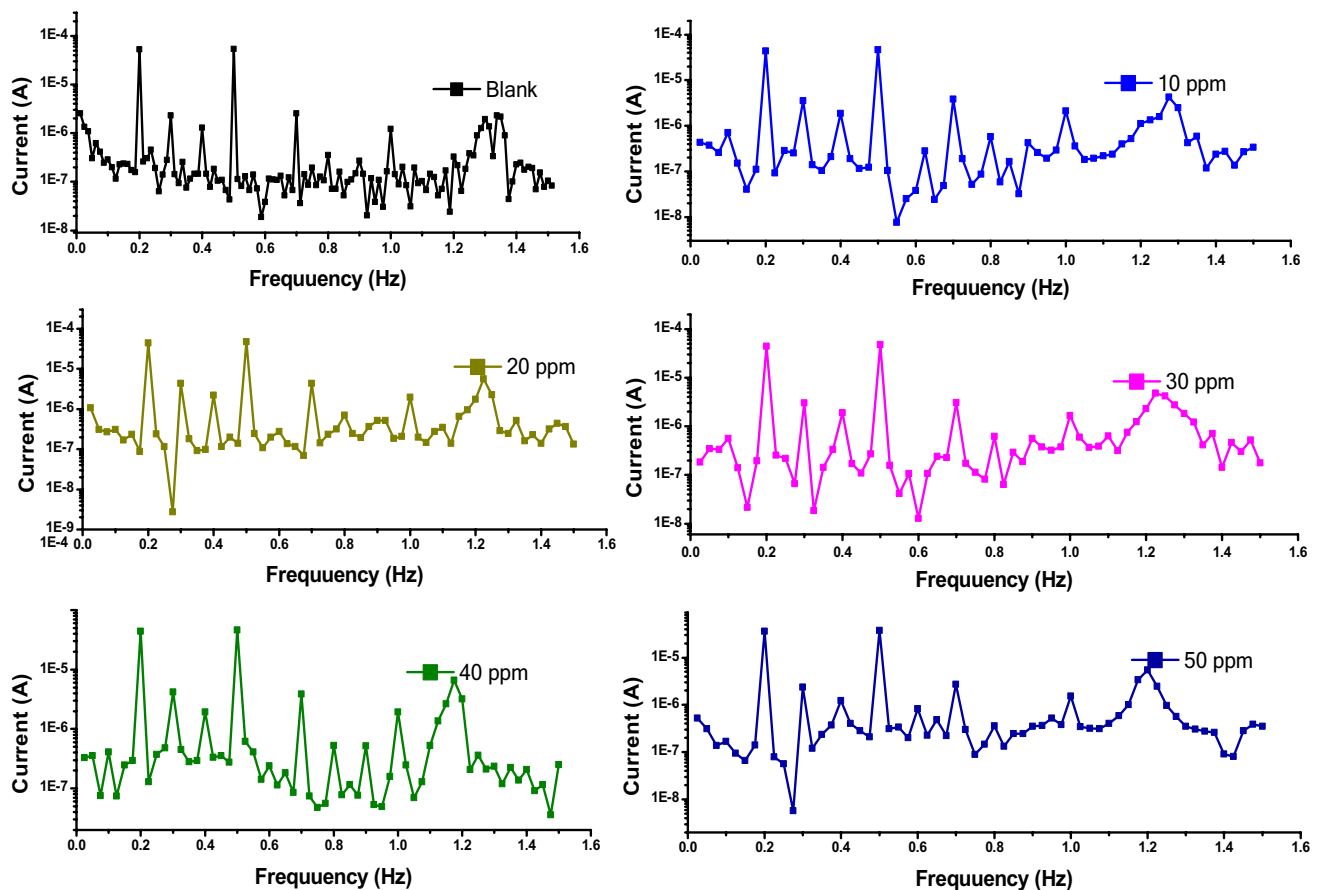


Fig. 11 EFM diagrams for the dissolution of C-steel in 1 M HCl in the attendance and absence of altered doses of amide compound (1) at  $30\text{ }^\circ\text{C}$

**Table 10** EFM data for the corrosion of C-steel in 1 M HCl in the presence and absence of altered doses of amide compound (1) at 30 °C

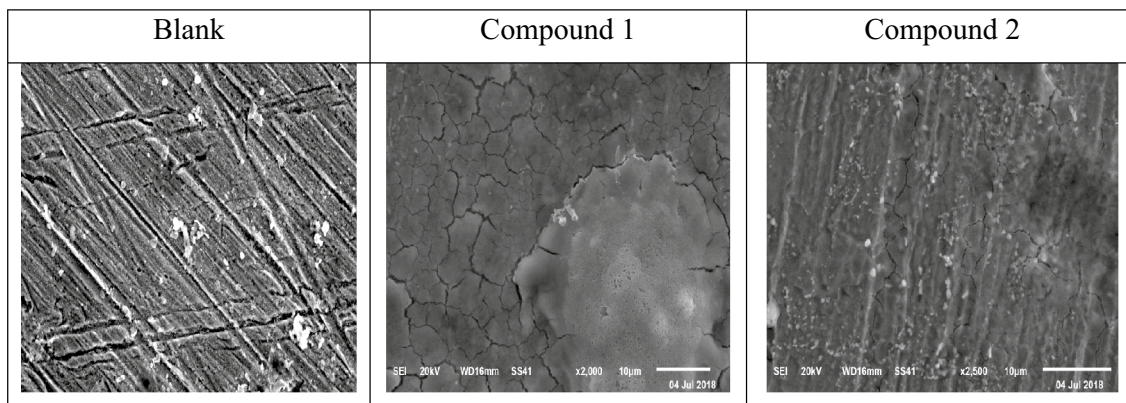
Conc. $\mu\text{M}$	$i_{\text{corr}}$ $\mu\text{A cm}^{-2}$	$\beta_a$ $\text{mV dec}^{-1}$	$\beta_c$ $\text{mV dec}^{-1}$	C.R. mpy	CF-2	CF-3	$\Theta$	%IE	
1 M HCl	552.4 $\pm$ 0.44	90 $\pm$ 0.49	99 $\pm$ 0.46	254.1	1.92	2.71	–	–	
Compound 1	10	295.1 $\pm$ 0.31	9 $\pm$ 0.060	100 $\pm$ 0.60	135.21	1.72	2.81	0.465	41.5
	20	199.9 $\pm$ 0.42	84 $\pm$ 0.51	100 $\pm$ 0.60	92.13	1.83	3.21	0.638	63.8
	30	108.1 $\pm$ 0.23	65 $\pm$ 0.70	72 $\pm$ 0.52	50.12	1.99	3.13	0.804	80.4
	40	101.9 $\pm$ 0.33	87 $\pm$ 0.52	123 $\pm$ 0.46	46.22	1.98	2.99	0.815	81.5
	50	72.11 $\pm$ 0.51	67 $\pm$ 0.53	78 $\pm$ 0.49	32.81	1.92	2.91	0.869	86.9
Compound 2	10	323.1 $\pm$ 0.35	97 $\pm$ 0.44	104 $\pm$ 0.52	147.92	1.91	2.85	0.415	41.5
	20	175.1 $\pm$ 0.44	88 $\pm$ 0.32	111 $\pm$ 0.29	126.11	1.89	3.22	0.501	50.1
	30	202.9 $\pm$ 0.18	101 $\pm$ 0.47	126 $\pm$ 0.34	93.11	2.03	3.11	0.632	63.2
	40	131.2 $\pm$ 0.21	77 $\pm$ 0.21	92 $\pm$ 0.31	59.93	1.83	3.09	0.762	76.2
	50	72.11 $\pm$ 0.35	112 $\pm$ 0.26	118 $\pm$ 0.42	45.95	2.01	2.98	0.818	81.8

values increase as electron donation of inhibitor molecules to empty metal *d*-orbitals and adsorption increases, but the lower values of ELUMO the easier to inhibitor to accept an electron from a metal surface. The gap in the energy band ( $\Delta E = \text{ELUMO} - \text{EHOMO}$ ), which is the energy to eliminate an electron from the last orbital occupied, influence the efficiency of inhibition. The higher  $\Delta E$  values of an inhibitor, the lower its efficiency because the ionization potential will be high, and the energy required to eliminate an electron from the outer occupied orbital will be high [56]. EHOMO values are in the order compound (1) > compound (2) which suggest the electron donation of compound (1) is the highest and so adsorb on CS surface to great extent, but ELUMO values are in reverse order. When the global hardness increases, the reactivity increases and so decreases the inhibition ability inhibitor. The results show that the compound (1) has lower value of the hardness ( $\eta$ ) value. On the other hand,  $X$  values will decrease when increasing the inhibition effectiveness. The values of ( $X$ ) and ( $\sigma$ ) softness of the inhibitor are recorded in Table 12. It is well-known that hard compounds possess

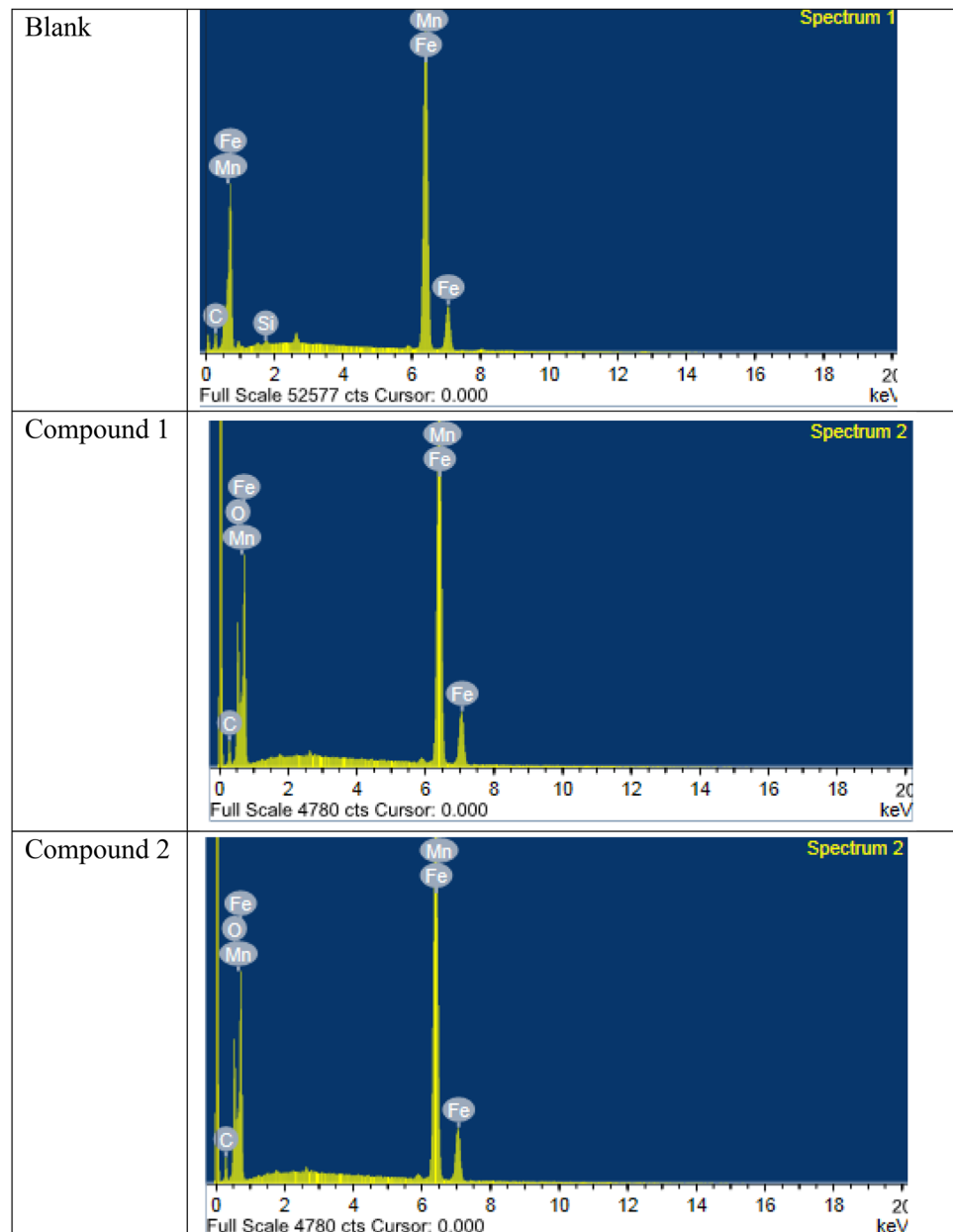
a large HOMO–LUMO gap [57] and metals and its alloys are known as soft acids so effective metal inhibitors should be as soft bases. So, compound (1) which possess the lowest  $\Delta E$  (highest softness) possess the highest value of inhibition efficiency [58, 59]. The ( $\mu$ ) calculated the polarity with the covalent bond between the compounds studied. It is accepted that the high  $\mu$  values improve the adsorption tendency on metal surface of the compounds tested, so, compound (1) > compound (2) (Table 12).

### 3.9 Monte Carlo (MC) simulation

The side and top observations of the most suitable adsorption formations for the amide unprotonated compounds and protonated tested on the C-steel surface obtained from the adsorption locator module are thus shown in Figs. 18 and 19 respectively. Adsorption energy is characterized as declining energy, when two materials are mixed during the adsorption process in which an electron, ion or molecule (adsorbent) is bound to the solid surface. As seen in Tables 13 and 14 compound (1) has higher energy

**Fig. 12** Micrographs of samples with and without inhibitors

**Fig. 13** EDX spectra of c-steel samples without and with inhibitors



for adsorption relative to compound (2), which predicts the heavy adsorption of compound (1) Niclosamide on the hardened surface of C-steel creating adsorbed stable layers which protecting the C-steel from corrosion. Compound (1) > compound (2).

### 3.9.1 Mechanism of corrosion inhibition

Inhibition of C-steel corrosion by investigated compounds is mainly due to its adsorption physically or chemically on the metal surface by replacing H<sub>2</sub>O molecules from the steel surface and creating a compact barrier film [60]. In

case of physical adsorption, electrostatic interaction occurs between charges metal surface and charged inhibitor molecules. While in chemical adsorption, pair electron on the heteroatoms (N, O),  $\pi$ -electron of multiple bonds as well as phenyl group with vacant *d*-orbitals of iron [61, 62]. As in present case the values of  $\Delta G_{\text{ads}}$  are ranging between 25.6 and 27.2 kJ mol<sup>-1</sup>, which indicates that investigated compound molecules are adsorbed by combination of both physical and chemical. It is known experimentally that steel surface is positively charged in acidic solutions, so, initially Cl<sup>-</sup> ions may get adsorbed on positively charged steel surface (Fig. 20), and then adsorption of the

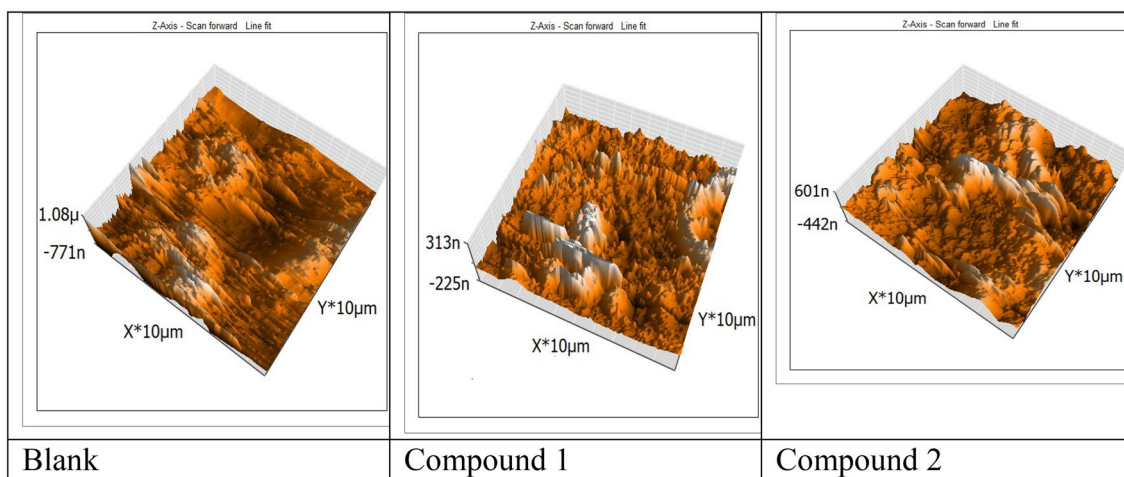


**Fig. 14** 3D AFM images of C-steel samples surface with and without inhibitors

**Table 11** AFM data for C-steel in 1.0 M HCl and with 50 µM of compound 1 and 2

Parameters	Blank	Compound 1	Compound 2
The roughness average (Sa)	202.39 nm	61.941 nm	116.45 nm
The mean value (Sm)	-10.334 nm	-14.252 nm	-9.6192 nm
The root mean square (Sq)	259.52 nm	90.43 nm	147.23 nm
The valley depth (Sv)	-1423.7 nm	-920.01 nm	-622.47 nm
The peak height (Sp)	1167.9 nm	656.08 nm	721.27 nm
The peak-valley height (Sy)	2591.6 nm	1576.1 nm	1343.7 nm

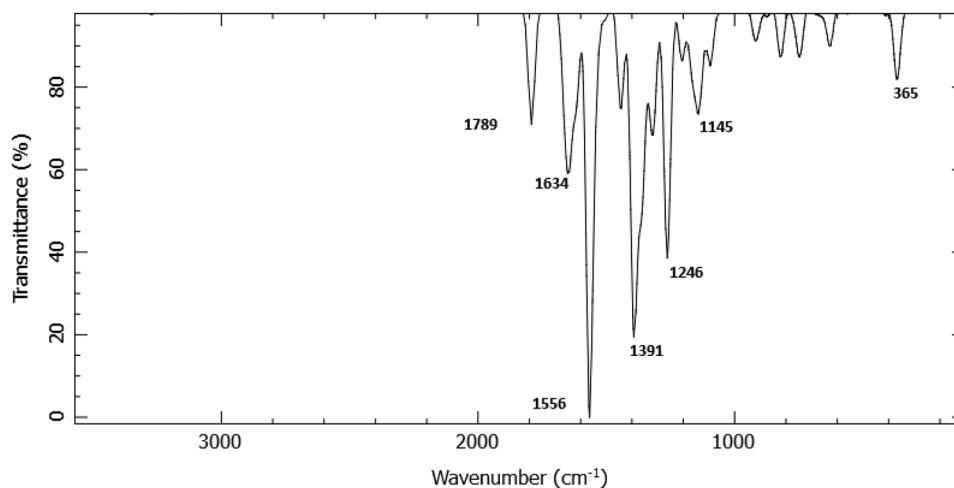
protonated inhibitor molecules occurs via electrostatic attraction (physical adsorption). But at the same time lone pair of electrons on heteroatoms,  $\pi$ -electron of benzene ring are donated to 3d-orbitals of iron atoms. (Chemical

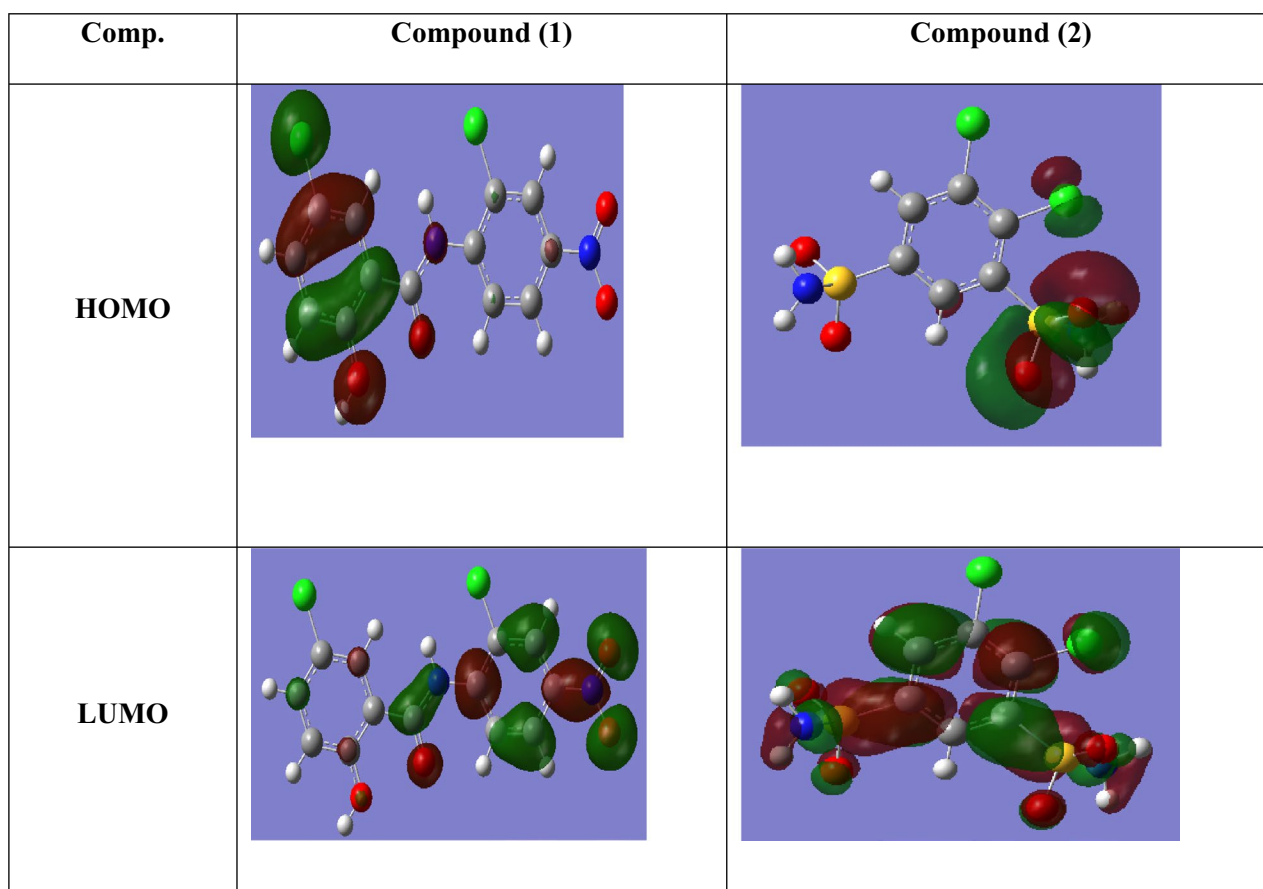
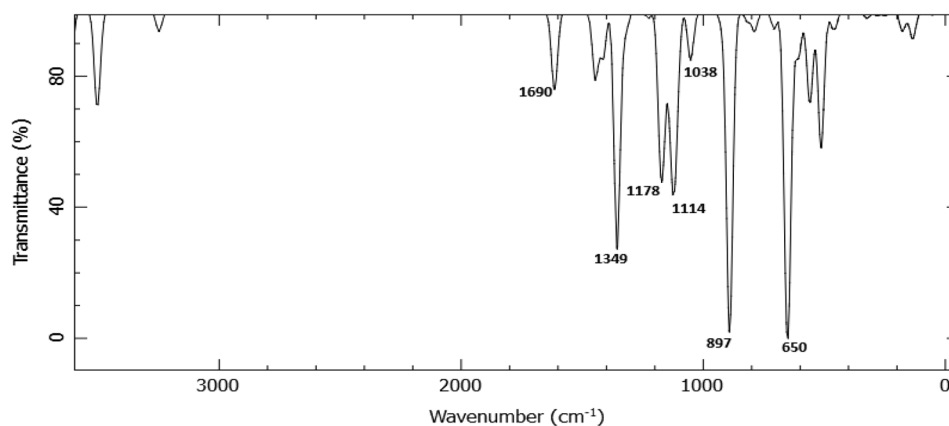
adsorption). Also, the filled 4s-orbitals can give their electrons to LUMO of the inhibitor's molecules via reterodonation. Niclosamide (comp. 1) > Dichlorphenamide (comp.2) in inhibition efficiency as recorded in all test methods and in the theoretical calculations also, this due to: a) larger molecular size which cover more surface area 2) It contains two benzene rings.

## 4 Conclusions

The amide compounds investigated have a high inhibition efficiency ranging from 96 and 97% at 50 µM based on measurements of MR as it gives linear variation of MR over time. %IE increased with amide compounds dose. PP measurements show that these investigated compounds inhibited the corrosion process by means of mixed-type inhibition, affecting both hydrogen evolution and metal

**Fig. 15** FT-IR spectrum of compound (1)



**Fig. 16** FT-IR spectrum of compound (2)**Fig. 17** The frontier molecular orbital density distribution for LMAEO-30 and LMAEO-9 investigated surfactants (HOMO and LUMO)**Table 12** Quantum parameters for the studied comp. (1) and comp. (2)

Comp	EHOMO (ev)	ELUMO (ev)	$\Delta E$ (ev)	$\eta = \Delta E/2$	$\sigma = 1/\eta$	$\Pi = (EHOMO + ELUMO)/2$ (ev)	$X = -\Pi$	Dipole moment (Debye)
(1)	-0.276	-2.674	2.398	1.199	0.834	-1.475	1.475	3.9604
(2)	-1.204	-5.599	4.395	2.1975	0.455	-3.4015	3.4015	1.9352

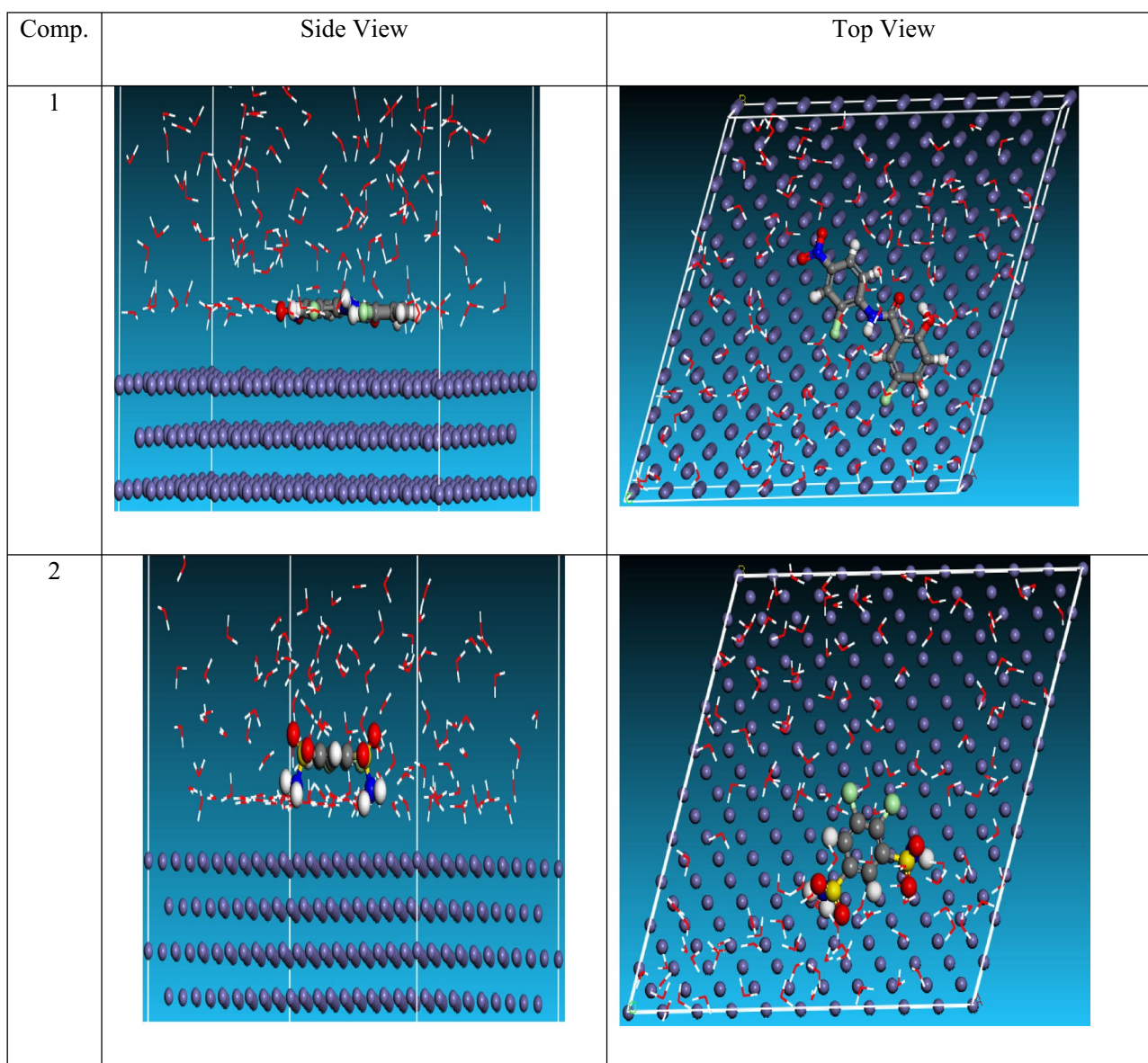


**Fig. 18** The most appropriate conformation for adsorption of the compound (1) Niclosamide and compound (2) Dichlorophenamide molecules on Fe (110)

dissolution. EIS revealed that these compounds inhibited the corrosion process by adsorption on the metal/solution interface. The investigated compounds adsorbed mainly physically on C-steel surface and obeyed Langmuir isotherm. DFT-based quantum chemical computation of

parameters of investigated compounds confirmed their inhibiting potential, which was further corroborated by molecular dynamic modeling of these compounds onto the metal surface.



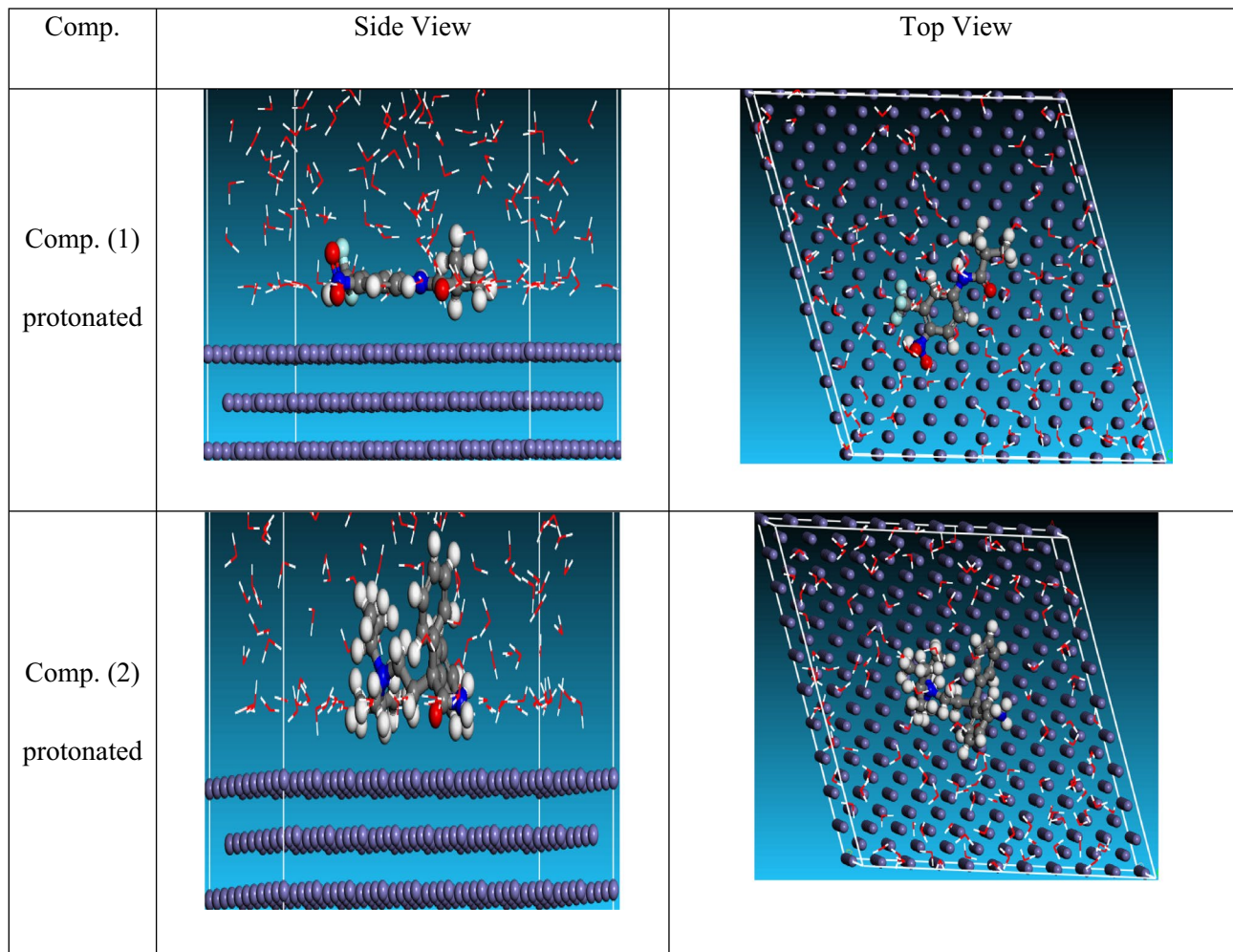


**Fig. 19** The most appropriate conformation for adsorption of the protonated comp. (1) Niclosamide and comp. (2) Dichlorphenamide molecules on Fe (110)

**Table 13** Results and descriptors measured by the Monte Carlo simulation for adsorption of amide compounds molecules on iron (110)

Structures	Total energy	Adsorption energy	Rigid adsorption energy	Deformation energy	Compound dEad/dNi	H <sub>2</sub> O dEad/dNi
Fe (110)/Niclosamide /H <sub>2</sub> O	-3153.04	-3153.021	-3312.492	159.47	-185.38	-7.03
Fe (110)/Dichlorphenamide /H <sub>2</sub> O	-3200.9	-3078.932	-3238.857	159.92	-50.50	-8.13

**Table 14** Results and descriptors measured by the Monte Carlo simulation for adsorption of protonated amide compound molecules on iron (110)

Structures	Total energy	Adsorption energy	Rigid adsorption energy	Deformation energy	Compound dEad/dNi	H <sub>2</sub> O dEad/dNi
Fe (110)/Flutamide protonated/H <sub>2</sub> O	-3.144	-3.124	-3.279	155.03	-134.17	-6.83
Fe (110)/Isopropamide protonated/H <sub>2</sub> O	-3.131	-3.143	-3.309	166.04	-135.92	-7.90

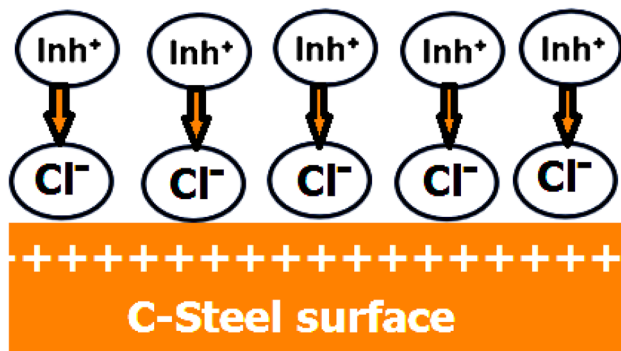


Fig. 20 Mechanism of corrosion inhibition

## Compliance with ethical standards

**Conflict of interest** The author declares that they have no conflict of interest.

**Open Access** This article is licensed under a Creative Commons Attribution 4.0 International License, which permits use, sharing, adaptation, distribution and reproduction in any medium or format, as long as you give appropriate credit to the original author(s) and the source, provide a link to the Creative Commons licence, and indicate if changes were made. The images or other third party material in this article are included in the article's Creative Commons licence, unless indicated otherwise in a credit line to the material. If material is not included in the article's Creative Commons licence and your intended use is not permitted by statutory regulation or exceeds the permitted use, you will need to obtain permission directly from the copyright holder. To view a copy of this licence, visit <http://creativecommons.org/licenses/by/4.0/>.

## References

- Liao LL, Mo S, Lei JL, Lei LHQ, Bing N, Li NB (2016) Application of a cosmetic additive as an eco-friendly inhibitor for mild steel corrosion in HCl solution. *J Coll Interface Sci* 474:68–77. <https://doi.org/10.1016/j.jcis.2016.04.015>
- Raja PB, Sethuraman MG (2008) Natural products as corrosion inhibitor for metals in corrosive media—a review. *Mat Lett* 62:113–116. <https://doi.org/10.1016/j.matlet.2007.04.079>
- Fouda AS, Elwakeel AM, Shalabi K, Elhossiany A (2015) Corrosion inhibition for carbon steel by levofloxacin drug in acidic medium. *J Elixir Corros Dye* 83:33086–33094
- Elhamdani N, Fdil R, Tourabi M, Jama C, Bentiss F (2015) Alkaloids extract of *Retama monosperma* (L.) boiss seeds used as novel eco-friendly inhibitor for carbon steel corrosion in 1 M HCl solution: electrochemical and surface studies. *Appl Surf Sci* 357:1294–1305. <https://doi.org/10.1016/j.apsusc.2015.09.159>
- Fouda AS, Shalabi K, El-Hossiany A (2016) Moxifloxacin antibiotic as green corrosion inhibitor for carbon steel in 1M HCl. *J Bio Tribo Corros* 2:18. <https://doi.org/10.1007/s40735-016-0048-x>
- Fouda AS, El-Azaly AH, Awad RS, Ahmed AM (2014) New benzonitrile azo dyes as corrosion inhibitors for carbon steel in hydrochloric acid solutions. *Int J Electrochem Sci* 9:1117–1131
- Fouda AS, Etaiw SH, Wahba A (2015) Effect of acetazolamide drug as corrosion inhibitor for carbon steel in hydrochloric acid solution. *Nat Sci* 13(9):1–8
- Fouda AS, El-Hossiany A, Ramadan H (2017) Calotropis procera plant extract as green corrosion inhibitor for 304 stainless steel in hydrochloric acid solution. *Zastita Materijala* 58(4):541–555
- Fouda AS, EL-Ewady G, Ali AH (2017) Modazar as promising corrosion inhibitor of carbon steel in hydrochloric acid solution. *Green Chem Lett Rev* 10(2):88–100. <https://doi.org/10.1080/17518253.2017.1299228>
- Fouda AS, Ibrahim H, Rashwan S, El-Hossiany A, Ahmed RM (2018) Expired drug (pantoprazole sodium) as a corrosion inhibitor for high carbon steel in hydrochloric acid solution. *Int J Electrochem Sci* 13:6327–6346. <https://doi.org/10.20964/2018.07.33>
- Said MT, Ali SA, Rahman SU (2003) The cyclic hydroxyl amines: a new class of corrosion inhibitors of carbon steel in acidic medium. *Anti-Corros Methods Mater* 50:201–207. <https://doi.org/10.1108/00035590310471778>
- Fouda AS, Eissa M, El-Hossiany A (2018) Ciprofloxacin as eco-friendly corrosion inhibitor for carbon steel in hydrochloric acid solution. *Int J Electrochem Sci* 13:11096–11112. <https://doi.org/10.20964/2018.11.86>
- Tamilselvi S, Rajeswari S (2003) The effect of triazoles and surfactants on the corrosion inhibition of carbon steel in acid solution. *Anti-Corros Methods Mater* 50:223–231. <https://doi.org/10.1108/00035590310471804>
- Keera ST (2003) The beneficial influence of halide ions on the inhibition characteristics of nitrogen-containing organic inhibitors to reduce the corrosion rate of carbon steel in HCl. *Anti-Corros. Methods Mater* 50:280–285. <https://doi.org/10.1108/00035590310482514>
- Bentiss F, Lagrenée M, Traisnel M, Hornez JC (1999) The corrosion inhibition of mild steel in acidic media by a new triazole derivative". *Corros Sci* 41:789–803. [https://doi.org/10.1016/S0010-938X\(98\)00153-X](https://doi.org/10.1016/S0010-938X(98)00153-X)
- Bentiss F, Traisnel M, Lagrenée M (2001) Influence of 2,5-bis(4-dimethylaminophenyl)-1,3,4-thiadiazole on corrosion inhibition of mild steel in acidic media. *J Appl Electrochem* 31:41–48
- Bendaif H, Melhaoui A, Azzouzi M El, Legssyer B, Hamat T, Elyoussfi A, Aouniti AE, Ouadi Y, Aziz M (2016) Eco-friendly *pancratium foetidum* pom extracts as corrosion inhibitors for mild steel in 1M HCl media. *J Mater Environ Sci* 7:1276–1287
- Bentiss F, Lagrenée M (2011) Heterocyclic compounds as corrosion inhibitors for mild steel in hydrochloric acid medium—correlation between electronic structure and inhibition efficiency. *J Mater Environ Sci* 2:13–17
- Verma C, Olasunkanmi LO, Ebenso EE, Quraishi MA, Obot IB (2016) Heterocyclic compounds as corrosion inhibitors for mild steel in hydrochloric acid medium—correlation between electronic structure and inhibition efficiency. *J Phys Chem C* 120:11598–11611
- Verma C, Olasunkanmi OIB, Ebenso EE, Quraishi MA (2016) 2,4-Diamino-5-(phenylthio)-5H-chromeno [2,3-b] pyridine-3-carbonitriles as green and effective corrosion inhibitors: gravimetric, electrochemical, surface morphology and theoretical studies. *RSC Adv* 6:1–50
- Gece G (2011) Drugs: a review of promising novel corrosion inhibitors. *Corros Sci* 53:3873–3898. <https://doi.org/10.1016/j.corsci.2011.08.006>
- Fouda AS, Farahat MM, Abdallah M (2014) Cephalosporin antibiotics as new corrosion inhibitors for nickel in HCl solution. *Res Chem Intermed* 40:1249–1266. <https://doi.org/10.1007/s11164-013-1036-0>
- Binnig G, Quate CF, Gerber CH (1986) Atomic force microscope. *Phys Rev Lett* 56(9):930–933

24. Fouda AS, Abd El-Ghaffar MA, Sherif MH, El-Habab TA, El-Hossiany A (2020) Novel anionic 4-tert-octyl phenol ethoxylate phosphate surfactant as corrosion inhibitor for C-steel in acidic media. *Prot Metals Phys Chem Surf* 56(1):189–201. <https://doi.org/10.1134/S2070205120010086>
25. Ansari K, Quraishi M (2015) Experimental and quantum chemical evaluation of Schiff bases of isatin as a new and green corrosion inhibitor for mild steel in 20% H<sub>2</sub>SO<sub>4</sub>. *J Taiwan Inst Chem Eng* 54:145–154. <https://doi.org/10.1016/J.JTICE.2015.03.013>
26. Fouda AS, Al-Hazmi NE, El-Zehry HH, El-Hossainy A (2020) Electrochemical and surface characterization of chondria macrocarpa extract (CME) as save corrosion inhibitor for aluminum in 1M HCl medium. *J Appl Chem* 9(3):362–381
27. Bockris JO, Swinkels DAJ (1964) Adsorption of normal decylamine on solid metal electrodes". *J Electrochem Soc* 111:736–743
28. Oguzie EE, LiY WFH (2007) Effect of 2-amino-3-mercaptopropanoic acid (cysteine) on the corrosion behavior of low carbon steel in sulphuric acid. *Electrochim Acta* 53:909–914. <https://doi.org/10.1016/j.electacta.2007.07.076>
29. Mohamadi M, Tehrani-Bagha AR, Mahdavian M (2013) Effect of aging time on corrosion inhibition of cationic surfactant on mild steel in sulfamic acid cleaning solution. *Corros Sci* 70:46–56. <https://doi.org/10.1016/j.corsci.2013.01.007>
30. Fouda AS, Abd El-Maksoud SA, Belal AAM, El-Hossiany A, Ibrahim A (2018) Effectiveness of some organic compounds as corrosion inhibitors for stainless steel 201 in 1M HCl: experimental and theoretical studies. *Int J Electrochem Sci* 13:9826–9846. <https://doi.org/10.20964/2018.10.36>
31. Cook TR, Zheng YR, Stang PJ (2013) Metal-organic frameworks and self-assembled supramolecular coordination complexes: comparing and contrasting the design, synthesis, and functionality of metal-organic material. *Chem Rev* 113(1):734–777. <https://doi.org/10.1021/cr3002824>
32. Noor EA, AL-Moubaraki AH (2008) Thermodynamic study of metal corrosion and inhibitor adsorption processes in mild steel/1-methyl-4[4'(-X)-styryl] pyridinium iodides/hydrochloric acid systems. *Mater Chem Phys* 110(1):145–154
33. Li X, Deng S, Fu H, Li T (2009) Adsorption and inhibition effect of 6-benzylaminopurine on cold rolled steel in 1.0M HCl. *Electrochim Acta* 54(16):4089–4098. <https://doi.org/10.1016/j.electacta.2009.02.084>
34. Fouda AS, Abdel Azeem M, Mohamed SA, El-Hossiany A, El-Desouky E (2019) Corrosion inhibition and adsorption behavior of nerium oleander extract on carbon steel in hydrochloric acid solution. *Int J Electrochem Sci* 14:3932–3948. <https://doi.org/10.20964/2019.04.44>
35. Li WH, He Q, Zhang ST, Pei CL, Hou BR (2008) Some new triazole derivatives as inhibitors for mild steel corrosion in acidic medium. *J Appl Electrochem* 38:289–292. <https://doi.org/10.1007/s10800-007-9437-7>
36. Ferreira ES, Giancomelli C, Giancomelli FC, Sinelli A (2004) Evaluation of the inhibitor effect of L-ascorbic acid on the corrosion of mild steel. *Mater Chem Phys* 83:129–134. <https://doi.org/10.1016/j.matchemphys.2003.09.020>
37. Elayyachy M, Elkodadi M, Aouniti A, Ramdani A, Hammouti B, Malek F, Elidrissi A (2005) New bipyrazole derivatives as corrosion inhibitors for steel in hydrochloric acid solutions". *Mater Chem Phys* 93:281–285. <https://doi.org/10.1016/j.matchemphys.2005.03.059>
38. Motawea MM, El-Hossiany A, Fouda AS (2019) Corrosion control of copper in nitric acid solution using chenopodium extract. *Int J Electrochem Sci* 14:1372–1387. <https://doi.org/10.20964/2019.02.29>
39. El-Haddad MN, Fouda AS (2013) Corrosion inhibition and adsorption behavior of some azo dye derivatives on carbon steel in acidic medium: synergistic effect of halide ions". *Chem Eng Commun* 200:1366–1393. <https://doi.org/10.1080/00986445.2012.746675>
40. Fouda AEAS, El-Gharkawy ES, Ramadan H, El-Hossiany A (2021) Corrosion resistance of mild steel in hydrochloric acid solutions by clinopodium actions as a green inhibitor. *Biointerface Res Appl Chem* 11(2):9786–9803
41. HasanovR SM, Bilgiç S (2007) Electrochemical and quantum chemical studies of some Schiff bases on the corrosion of steel in H2SO4 solution. *Appl Surf Sci* 253(8):3913–3921. <https://doi.org/10.1016/j.apsusc.2006.08.025>
42. Şahin M, Gece G, Karçı F, Bilgiç SJJAE (2008) Experimental and theoretical study of the effect of some heterocyclic compounds on the corrosion of low carbon steel in 3.5% NaCl medium. *J Appl Electrochem* 38(6):809–815. <https://doi.org/10.1007/s10800-008-9517-3>
43. Khaled KF (2008) Molecular stimulation, quantum chemical calculations and electrochemical studies for inhibition of mild steel by triazoles *Electrochim. Acta* 53(9):3484–3492. <https://doi.org/10.1016/j.electacta.2007.12.030>
44. Behpour M, Ghoreishi SM, Salavati-Niasari M, Ebrahimi B (2008) Evaluating two new synthesized S-N Schiff bases on the corrosion of copper in 15% HCl. *Mater Chem Phys* 107:153–157. <https://doi.org/10.1016/j.matchemphys>
45. Quartarone G, Ronchin L, Vavasori A, Tortato C, Bonaldo L, Quararone G, Ronchin L, Vavasori A, Tortato C, Bonaldo L (2012) Inhibitive action of gramine towards corrosion of mild steel in deaerated 1.0M hydrochloric acid solutions. *Corros Sci* 64:82–89
46. Golestani G, Shahidi M, Ghazanfari D (2014) Electrochemical evaluation of antibacterial drugs as environment-friendly inhibitors for corrosion of carbon steel in HCl solution. *Appl Sur Sci* 308:347–362
47. Karthik G, Sundaravadivelu M (2016) Studies on the inhibition of mild steel corrosion in hydrochloric acid solution by atenolol drug. *Egyptian J Petrol* 25:183–191
48. Aldana-Gonzalez J, Espinoza-Vazquez A, Romero-Romo M, Uruchurtu-Chavarin J, Palomar-Pardave M (2019) Electrochemical evaluation of cephalothin as corrosion inhibitor for API 5L X52 steel immersed in an acid medium. *Arabian J Chem* 12:3244–3253
49. Verma C, Quraishi MA, Gupta NK (2016) 2-(4-[[4-Methyl-6-(1-methyl-1H-1, 3-benzodiazol-2-yl)-2-propyl-1H-1, 3-benzodiazol-1-yl] methyl] phenyl) benzoic acid as green corrosion inhibitor for mild steel in 1M hydrochloric acid, *Ain Shams Eng J*
50. Obot IB, Ebenso EE, Kabanda MM (2013) Metronidazole as environmentally safe corrosion inhibitor for mild steel in 0.5 M HCl: experimental and theoretical investigation. *J Environ Chem Eng* 1:431–439
51. Mohammed KZ, Hamdy A, Abbas M (2012) A pharmaceutically active compound as corrosion inhibitor for carbon steel in acidic medium: electrochemical and thermodynamic studies. *RJPBCS* 3(2):912–928
52. Singh A, Gupta A, Rawat AK, Ansari KR, Quraishi MA, Ebenso EE (2014) Cimetidine as an effective corrosion inhibitor for mild steel in hydrochloric acid. *Int J Electrochem Sci* 9:7614–7628
53. Akpan A, Offiong NO (2015) Electrochemical linear polarization studies of Amodiaquine drug as a corrosion inhibitor for mild steel in 0.1M HCl solution. *Chem Mater Res* 7:17–20
54. Eddy NO, Odoemelam SA, Mbaba AJ (2008) Inhibition of the corrosion of mild steel in HCl by sparfloxacin. *African J Pure Appl Chem* 2:132–138
55. Jebakumar Immanuel Edison T, Sethuraman MG (2013) Electrochemical investigation on adsorption of fluconazole at mild steel/HCl acid interface as corrosion inhibitor, *Inter J Corros*, 2013 1

56. Reza I, Ahmad E, Kareem F (2012) Corrosion inhibition mechanism of piperacillin sodium for mild steel protection in acidic media. *Afinidad LXVIII Enero Marzo* 557:47–51
57. Khan MZH, Aziz MA, Hasan MR, Al-Mamun MR (2016) The role of drug as corrosion inhibitor for mild steel surface characterization by SEM, AFM, and FTIR. *Anti-Corros Meth Mater* 63:308–315
58. Gilman AG, Rall TW, Nies AS, Taylor P (1990) (Eds) Goodman and Gilman's. In: *The pharmacological basis of therapeutics*. 8th ed. Pergamon Press: New York, pp. 965
59. Tawi LR, McDermott MP, Brown R Jr, Shapiro BC, Ptacek LJ, McManis PG, Dalakas MC, Spector SA, Mendell JR, Hahn AF, Griggs RC (2000) Randomized trials of dichlorphenamide in the periodic paralyses. Working group on periodic paralysis. *Ann Neurol* 47(1):46–53
60. Fouda AS, Abd El-Maksoud SA, El-Hossiany A, Ibrahim A (2019) Corrosion protection of stainless steel 201 in acidic media using novel hydrazine derivatives as corrosion inhibitors. *Int J Electrochem Sci* 14:6045–6064. <https://doi.org/10.20964/2019.03.15>
61. Saleh MM, Atia AA (2006) Effects of structure of the ionic head of cationic surfactant on its inhibition of acid corrosion of mild steel. *J Appl Electrochem* 36:899–905. <https://doi.org/10.1007/s10800-006-9147-6>
62. Ameh PO, Eddy NO (2014) Commiphora pendunculata gum as a green inhibitor for the corrosion of aluminum alloy in 0.1M HCl. *Res Chem Intermed* 40:2641–2649. <https://doi.org/10.1007/s11164-013-1117-0>

**Publisher's Note** Springer Nature remains neutral with regard to jurisdictional claims in published maps and institutional affiliations.